Epoxy Nanocomposites with Two-Dimensional Transition Metal Dichalcogenide Additives

Osman Eksik,[†] Jian Gao,[‡] S. Ali Shojaee,[§] Abhay Thomas,[†] Philippe Chow,[‡] Stephen F. Bartolucci,[⊥] Don A. Lucca,[§] and Nikhil Koratkar[†,‡,*]

[†]Department of Mechanical, Aerospace and Nuclear Engineering, Rensselaer Polytechnic Institute, Troy, New York 12180, United States, [‡]Department of Materials Science and Engineering, Rensselaer Polytechnic Institute, Troy, New York 12180, United States, [§]School of Mechanical and Aerospace Engineering, Oklahoma State University, 218 Engineering North, Stillwater, Oklahoma 74078, United States, and [⊥]U.S. Army Armaments Research Development and Engineering Center, Benét Laboratories, Watervliet, New York 12189, United States

ABSTRACT Emerging two-dimensional (2D) materials such as transition metal dichalcogenides offer unique and hitherto unavailable opportunities to tailor the mechanical, thermal, electronic, and optical properties of polymer nanocomposites. In this study, we exfoliated bulk molybdenum disulfide (MoS_2) into nanoplatelets, which were then dispersed in epoxy polymers at loading fractions of up to 1% by weight. We characterized the tensile and fracture properties of the composite and show that MoS_2 nanoplatelets are highly effective at enhancing the mechanical properties of the epoxy at very low nanofiller loading fractions (below 0.2% by weight). Our results show the potential of 2D sheets of transition metal dichalcogenides as reinforcing additives in polymeric composites. Unlike graphene, transition metal dichalcogenides such as MoS_2 are high band gap semiconductors and do not impart significant electrical conductivity to the epoxy matrix. For many applications, it is essential to enhance mechanical properties while also maintaining the electrical insulation properties and the high dielectric constant of the polymer material. In such applications, conductive carbon based fillers such as graphene cannot be utilized. This study demonstrates that 2D transition metal dichalcogenide additives offer an elegant solution to such class of problems.

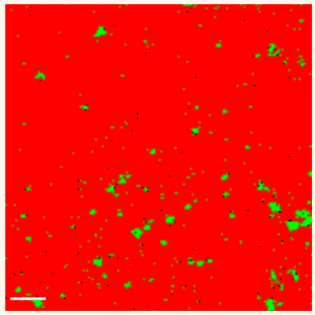

KEYWORDS: transition metal dichalcogenides · molybdenum disulfide · epoxy nanocomposites · mechanical properties · modulus · tensile strength · fracture toughness

Over the past decade there has been intense activity[1−11] in trying to reinforce polymer materials with nanoscale fillers to improve their mechanical, electrical, and thermal properties for a variety of engineering applications. The nanofillers that have been investigated include nanoparticles (*e.g.*, silica, alumina, titania, *etc.*),[1,2] one-dimensional (1D) nanostructures such as carbon nanotubes,[3,4] and two-dimensional (2D) nanofillers such as nanoclays[5−7] and more recently graphene.[8−11] While 2D nanofillers such as graphene have proven to be highly effective[10,11] in reinforcing polymer matrices, they are electrically conductive which limits their utility in many applications such as electric motors, electronics packaging, transmission lines, power electronics, capacitors, and electric field grading materials to name a few. For the aforementioned applications, it is critical to enhance mechanical properties while also maintaining the electrical insulation properties and the high dielectric constant of the polymer material. In such applications, conductive carbon fillers such as graphene or carbon nanotubes cannot be employed. Silica nanoparticles are commonly used in such situations, but they lack the effectiveness of 2D fillers such as graphene.

The recent interest and excitement in graphene has also opened up[12−16] a pandora's box of new 2D materials and material combinations which are now beginning to come to the fore. The most interesting and exciting of these emerging 2D materials are possibly transition metal dichalcogenides (TMDCs)[14−16] such as molybdenum disulfide (MoS_2) and tungsten disulfide (WS_2). As high band gap semiconductors, these materials will not impart electrical conductivity to the polymer matrix while at the same time potentially improving mechanical properties such as elastic modulus, strength, toughness,

* Address correspondence to koratn@rpi.edu.

Received for review March 11, 2014 and accepted April 22, 2014.

Published online April 22, 2014
10.1021/nn5014098

wear, creep and fatigue resistance. While the shock-absorbing performance of WS_2 and MoS_2 cage-like nanoparticles and their tribological applications as solid-state lubricants have been reported,[17,18] to our knowledge the mechanical properties of polymer materials reinforced by nanosheets of TMDCs have yet to be investigated in depth. In this study, we exfoliated bulk MoS_2 into nanoplatelets, which were then dispersed in epoxy polymers at loading fractions of up to 1% by weight. We characterized the tensile and fracture properties of the composite and show that MoS_2 nanoplatelets are highly effective at enhancing the mechanical properties of the epoxy at very low nanofiller loading fractions (~0.2% by weight). These results indicate that 2D sheets of transition metal dichalcogenides show significant potential as reinforcing additives in polymeric composites.

RESULTS AND DISCUSSION

Nanosheets of TMDCs such as MoS_2 or WS_2 can be synthesized using two basic approaches: (1) bottom-up synthesis by chemical vapor deposition[15,16] or (2) top-down synthesis by exfoliation of their bulk counterparts.[14] For composites applications, we require bulk quantities of TMDCs for which top-down exfoliation is far more scalable and cost-effective. To achieve such top-down exfoliation,[14] we examined the feasibility of ultrasonication of bulk TMDC powders which are commercially available. Since MoS_2 is significantly lighter[14] than WS_2, we decided to focus our efforts on MoS_2-based composites. Exfoliation of bulk MoS_2 powders was achieved by ultrasonication in a solvent (1-vinyl-2 pyrrolidone) for ~48 h in a low power sonic bath (Branson CPX-952-516R, 40 kHz). The concentration of MoS_2 powder in the solvent was ~5 mg/mL. The solution was then centrifuged at ~4000 rpm for ~30 min and the supernatant was decanted immediately. Figure 1a shows a typical scanning electron microscopy (SEM) image of MoS_2 nanoplatelets (MNP) synthesized by the above approach and deposited on to a silicon wafer for imaging. Raman spectra of the MNP (Figure 1b) shows modes at ~382 cm^{-1} (the E^1_{2g} mode corresponding to in-plane vibrations) and at ~408 cm^{-1} (the A_{1g} mode that corresponds to out-of-plane vibrations) which are characteristic modes[16] of the trigonal prismatic structure of MoS_2. To determine the average MNP thickness, we performed atomic force microscopy (AFM) scans as shown in Figures 1c,d. The thickness of the MNP platelets ranges from 5 to 10 nm, which indicates that the above exfoliation method does not result in monolayer MoS_2. Similar AFM scans (not shown here) for monolayer chemical vapor deposited[16] MoS_2 sheets gave a thickness of ~1 nm. This indicates that the MNP in our study is composed of ~5−10 layers of MoS_2 with lateral (*i.e.*, in-plane) dimensions of about 400−500 nm.

The solution mixing process[19,20] used to disperse MoS_2 in epoxy is shown schematically in Figure 2a.

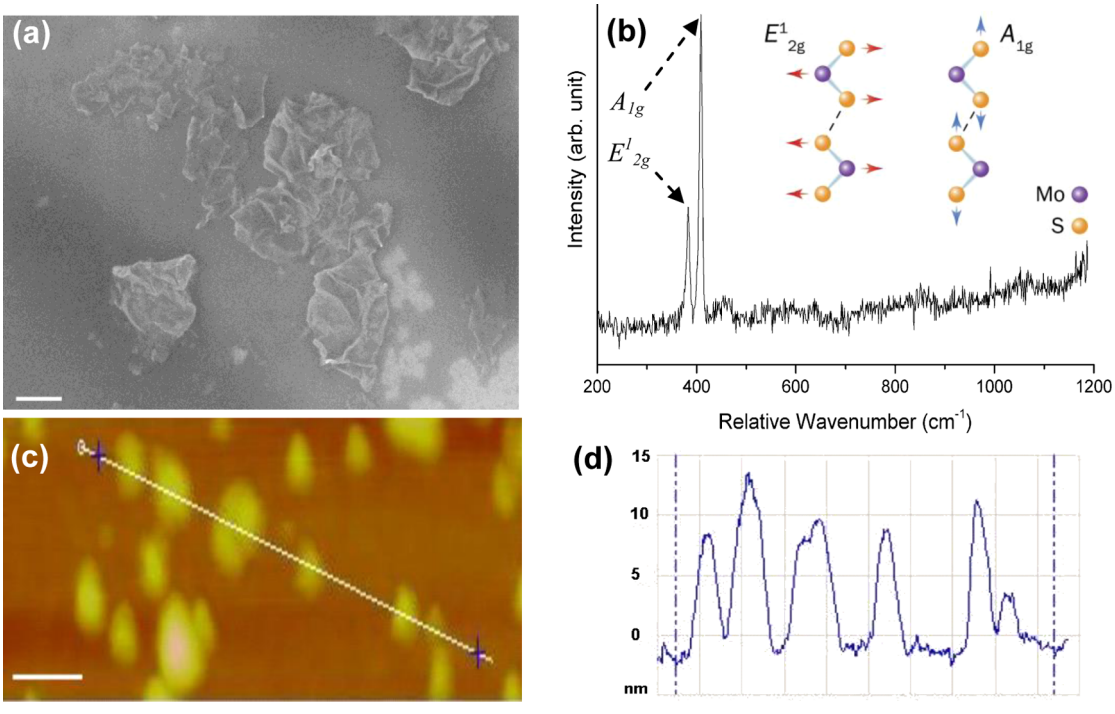

Figure 1. (a) Scanning electron microscopy image of wrinkled MoS_2 platelets (MNP) deposited on a silicon wafer. (b) Characteristic Raman spectra typical of MoS_2 acquired from the MNP. The E^1_{2g} mode that corresponds to in-plane vibrations and the A_{1g} mode corresponding to out-of-plane vibrations are marked out and the mode shapes are depicted schematically. (c and d) Atomic force microscopy scans indicating that the MNP are 5−10 nm in thickness and several hundred nanometers in lateral dimensions. Scale bar in (a) is 100 nm and in (c) is 500 nm.

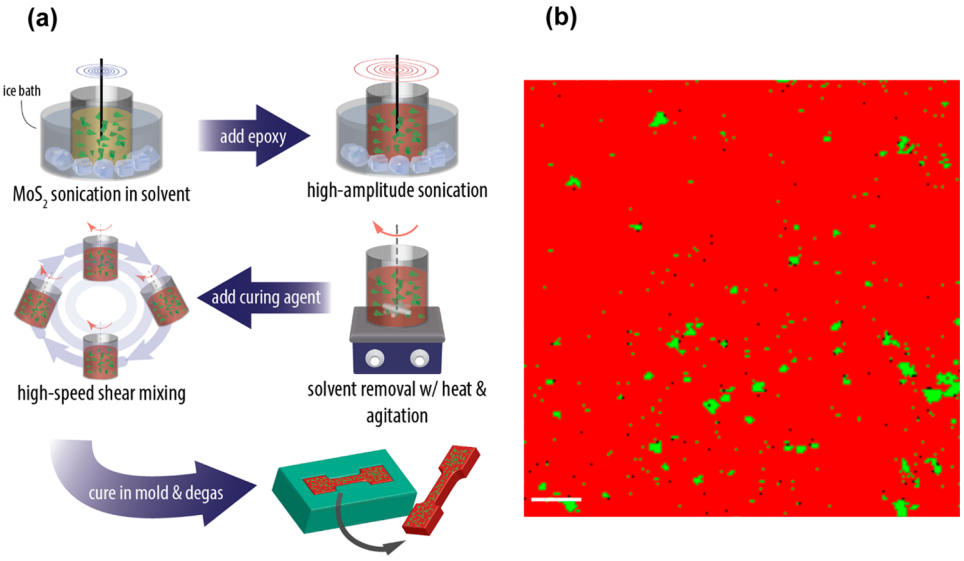

Figure 2. (a) Dispersion of MNP in an epoxy matrix by solution mixing (ultrasonication) and high speed shear blending. (b) Typical confocal Raman dispersion map showing distribution of MNP (green) sheets in the epoxy (red) matrix at an MNP loading fraction of ~0.2% by weight. The scale bar is 6 μm.

The epoxy resin (Epon 862: diglycidyl ether of bisphenol-F, Miller-Stephenson Chemical Co., Inc.) was added to a solution of MoS_2 Nano-Platelets (MNP) predispersed in an organic solvent (1-vinyl-2 pyrrolidone) and subjected to high amplitude ultrasonic (Sonics Vibra-cell VC 750 tip sonicator, power ~750 W, frequency ~20 kHz) agitation for ~12 h to uniformly mix the MNP and epoxy. Subsequently, the solvent was gradually removed through heating the mixture on a magnetic hot plate with stirring. After the MNP/epoxy mixture had cooled to room temperature, a low-viscosity curing agent (Epikure hardener, Miller-Stephenson Chemical Co., Inc.) was added, and a high-speed shear mixer (ARE-250, Thinky) was used to blend the MNP/epoxy slurry for ~4 min at ~2000 rpm. To remove any remaining air bubbles from the mixture, it was placed in a vacuum environment for ~30 min. Finally, silicone molds were used to cure the nanocomposite samples at room temperature for ~24 h followed by an overnight post cure at ~80 °C.

To quantify the dispersion of the MNP in the epoxy matrix, we used a confocal Raman imaging technique.[21,22] More specifically, we combined the measured Raman response of MNP (Figure 1b) with the capability of confocal Raman imaging to produce phase images to investigate the dispersion of MNP in the epoxy matrix. For Raman imaging, we created cross sections of the composites by slicing the composites with a low speed diamond saw. To obtain the confocal Raman images, a total of 32 400 individual spectra were collected over a 30 × 30 μm^2 area of the composite. The spatial variation of the integrated intensity over the spectral range of the A_{1g} Raman mode (Figure 1b) was used to map the dispersion of MNP in the composites. Figure 2b shows a typical dispersion map of MNP (green, indicating regions with high integrated intensity) in the epoxy matrix (red, indicating regions with low integrated intensity) for MNP loading of ~0.2% weight. The black dots in the Raman image represent intermediate intensities and are usually the result of artifacts (*i.e.*, cosmic rays) or very small MNPs. Figure 2b illustrates that confocal Raman imaging can be used to produce well-defined dispersion maps of the MNP in the polymer. The dispersion maps can also be used to quantify the average MNP size by dividing the total area in the image exhibiting MNP Raman modes by the number of agglomerates in the image. Then, assuming a circular geometry for the agglomerates, the average MNP size was estimated as ~420 nm which shows reasonable agreement with the SEM and AFM images of Figure 1a,c which indicate an average MNP size of ~400−500 nm.

Static tensile loading tests were performed on the MNP/epoxy nanocomposites using a MTS-858 material testing system following the ASTM D638 standard.[10] Figure 3a shows typical tensile stress *vs* strain plots for the baseline epoxy and MNP/epoxy nanocomposites with MNP weight fractions ranging from 0.1 to 1%. Figure 3b compares the Young's modulus of the pristine epoxy and the nanocomposite samples, and Figure 3c shows their ultimate tensile strength. The error bars represent the maximum and minimum values obtained. The results indicate that MNP fillers are effective at increasing the elastic modulus and the tensile strength of the epoxy at ultralow nanofiller loadings (0.1−0.2% by weight). However, beyond ~0.2% loading there is a reduction in performance and at ~1% loading the performance of the nanocomposite sample is comparable to the baseline epoxy. The reported results are the average of 5 different tests

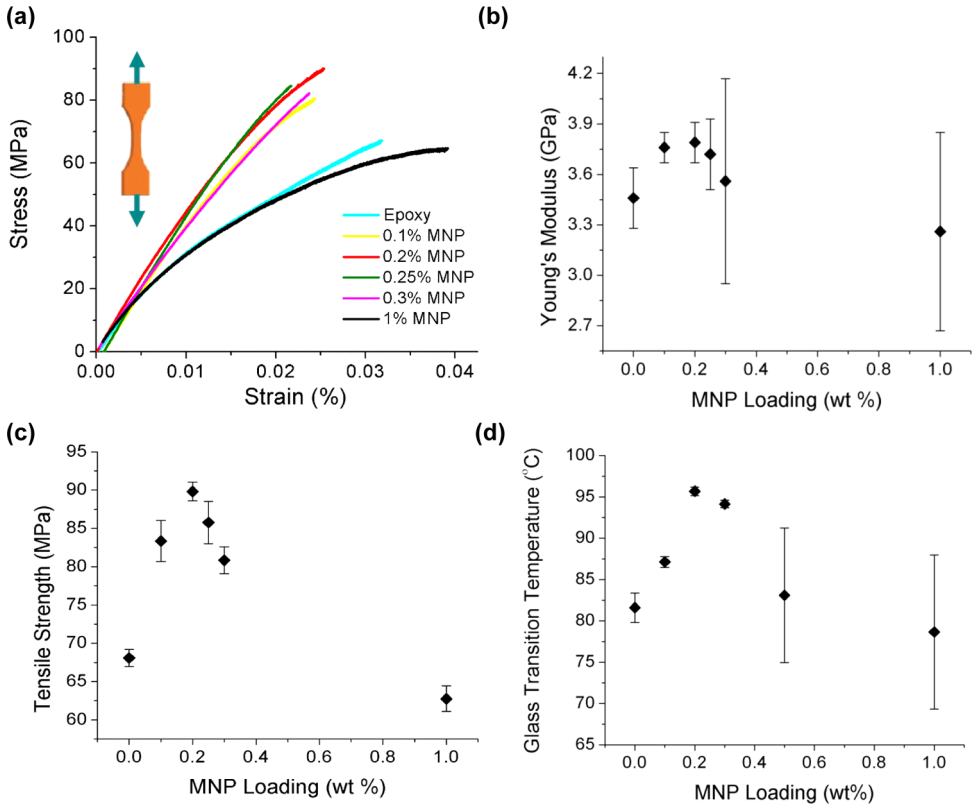

Figure 3. (a) Tensile properties (static stress *vs* strain response) of the MNP/epoxy nanocomposites. (b) Young's modulus *vs* MNP loading fraction. (c) Ultimate tensile strength *vs* MNP loading fraction. The elastic modulus and strength of the nanocomposites show a maximum at an MNP weight fraction of ~0.2%. (d) Measured glass transition temperature (T_g) *vs* MNP loading fraction showing a sharp increase in T_g up to an MNP weight fraction of ~0.2% beyond which the T_g drops back to the baseline epoxy value.

for each MNP loading fraction. Incorporation of nanofillers into a polymer matrix can also affect its glass transition temperature (T_g). To investigate this, we used differential scanning calorimetry (DSC) to measure the T_g of the baseline epoxy and nanocomposite samples. The results (Figure 3d) indicate that the T_g increases significantly for the lower weight fraction composites, from ~82 °C for the baseline (unfilled) epoxy to ~95 °C at ~0.2% MNP loading. For the higher weight loadings up to 1.0%, the T_g decreases to approximately that of the neat epoxy. Since the T_g is a thermal transition where polymer chain motion significantly increases, the increased T_g for the low weight fraction MNP nanocomposites is indicative of decreased chain mobility caused by interfacial interactions between the epoxy chains and the surfaces of the well dispersed MNP additives. Conversely, at the higher loading fractions, the MNP will likely form agglomerates, resulting in fewer interfacial interactions and the matrix mobility therefore returns toward the value of the neat epoxy. The trend seen in the T_g response (Figure 3d) corresponds well to those seen for the mechanical properties (Figure 3a–c).

Crack-opening tests were also performed (Figure 4a) on compact tension samples to measure the Mode I fracture toughness (K_{Ic}) of the pure epoxy matrix and the MNP/epoxy nanocomposites at various weight fractions of MNP. The tests were conducted using a MTS-858 material testing system following the ASTM standard D5045.[11] An initial precrack was created in the compact tension samples by gently tapping a fresh razor blade over a molded starter notch. The crack was then advanced by application of a force as shown in Figure 4a. At each weight fraction of MNP additives, five different samples were tested. Figure 4b shows that the K_{Ic} of the baseline epoxy (without MNP) is ~1 MPa $m^{1/2}$, which correlates well with published literature for epoxy materials. The addition of MNP into the epoxy matrix causes an increase in the nanocomposite K_{Ic} value to ~1.6 MPa $m^{1/2}$ at ~0.2% weight fraction of MNP, which corresponds to a ~60% increase in fracture toughness. For higher loading fractions, the enhancement in K_{Ic} diminishes and for an MNP weight fraction of ~1% the K_{Ic} reduces to ~1.25 MPa $m^{1/2}$. The maximum enhancement in K_{Ic} (~60% at 0.2% weight fraction of MNP) is impressive. To achieve similar increase (~62%) in K_{Ic}, the required weight fraction of SiO_2 nanoparticles[1] in epoxy was found to be ~14.8% which is ~74-fold larger than for MNP. Similarly, to obtain a ~65% increase in K_{Ic}, the loading fraction of Al_2O_3 (~5%) and TiO_2 (~10%) nanoparticles[2] in epoxy is ~25- to 50-fold larger than MNP.

In addition to the fracture toughness, the arithmetic mean roughness of the fracture surfaces was

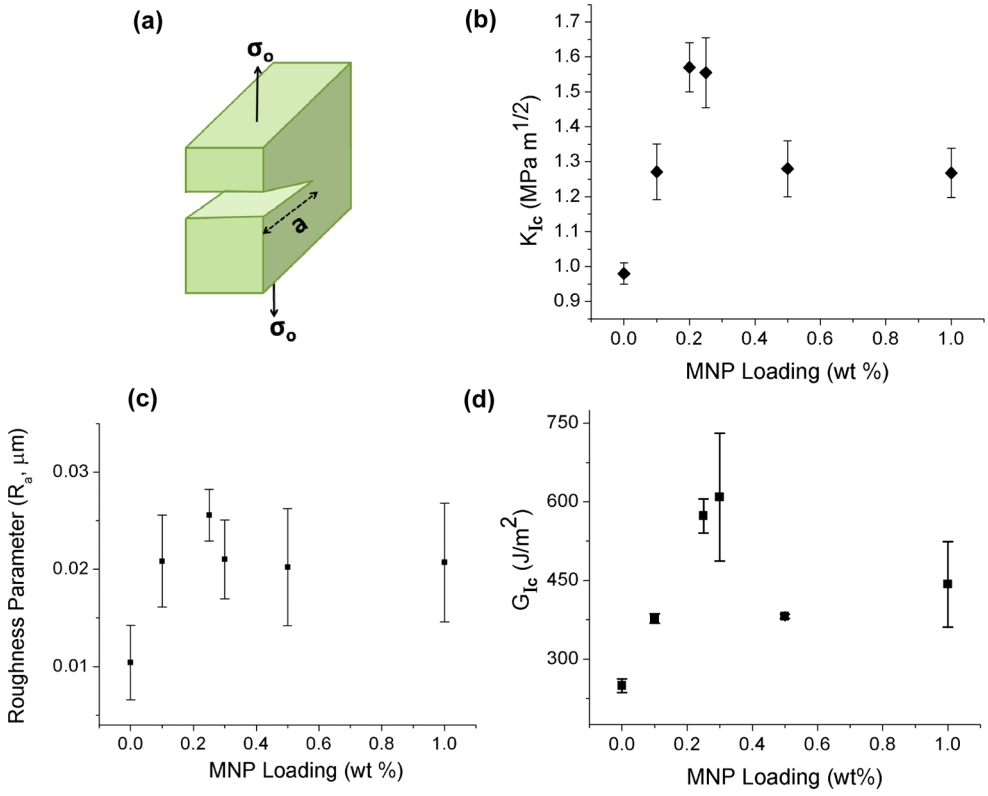

Figure 4. (a) Schematic of compact tension samples used for fracture toughness characterization. (b) Mode I fracture toughness plotted *vs* the MNP loading fraction. (c) Characterization of the roughness of the fracture surface *vs* the MNP loading content. (d) Mode I fracture energy plotted *vs* the MNP content.

measured. The data shown in Figure 4c are the average surface roughnesses for 5 separate measurements and indicate a ~150% increase in surface roughness as MNP content is increased from 0 to 0.3% by weight. This increase in roughness of the fracture surface with increase in MNP content suggests that crack deflection plays a significant role in the observed toughening. Crack deflection is the process by which an initial crack tilts and twists when it encounters a rigid inclusion such as the MNP. Crack deflections during crack propagation cause an increase in the total fracture surface area, resulting in greater energy absorption when compared to crack propagation without deflection. For crack deflection processes, an increase[23−25] in the fracture surface roughness with MNP loading is expected. This is the case for the 0−0.3% MNP weight fraction range, as indicated in Figure 4c. However, at higher weight fractions the fracture surface roughness is reduced as compared to the value at 0.3% MNP loading, which suggests deterioration in MNP dispersion at increased nanofiller loading content.

It should be noted that other forms of 2D fillers (such as intercalated nanoclays and graphene) have also proven to be effective in toughening epoxy systems. Graphene shows comparable performance[10,11] to MNP; however graphene cannot be used in applications where the electrical insulation and dielectric properties of the polymer need to be retained. For nanoclays, Zerda *et al.*[5] reported ~61% increase in the fracture toughness of the epoxy matrix for ~3.5% nanoclay weight fraction. Wang *et al.*[6] have achieved similar levels of enhancement (~78%) at ~2.5% weight fraction of nanoclay fillers. Liu *et al.*[7] have reported ~110% increase in K_{Ic} for an epoxy system with ~3% weight of nanoclay additives. It should be noted that these weight fractions are 10−15 times higher than the MNP weight fraction (~0.2%) in the present study. Moreover, in the case of nanoclay reinforced epoxy composites, the incorporation of nanoclays (in the range of 2.5−3.5% by weight) has been reported to cause a significant reduction in the tensile strength.[5,6] By contrast, the MNP additives were found to enhance the tensile strength by up to 40% in the 0.1−0.2% weight fraction range (Figure 3c). These results indicate that MNP additives are highly effective in strengthening and stiffening the epoxy matrix while also suppressing crack propagation and toughening the epoxy.

The measurement of elastic modulus (E) and fracture toughness (K_{Ic}) enables us to determine[11] the fracture energy of the nanocomposite: $G_{Ic} = K_{Ic}^2[(1 - \mu^2)/E]$, where μ is the Poisson's ratio. The fracture energy (G_{Ic}) quantifies the energy required to propagate the crack in the material. Figure 4d indicates that the G_{Ic} of the baseline epoxy (without the MNP) is ~230 J/m^2, which correlates well with the literature[23] for brittle polymers, which typically show relatively low values of G_{Ic}

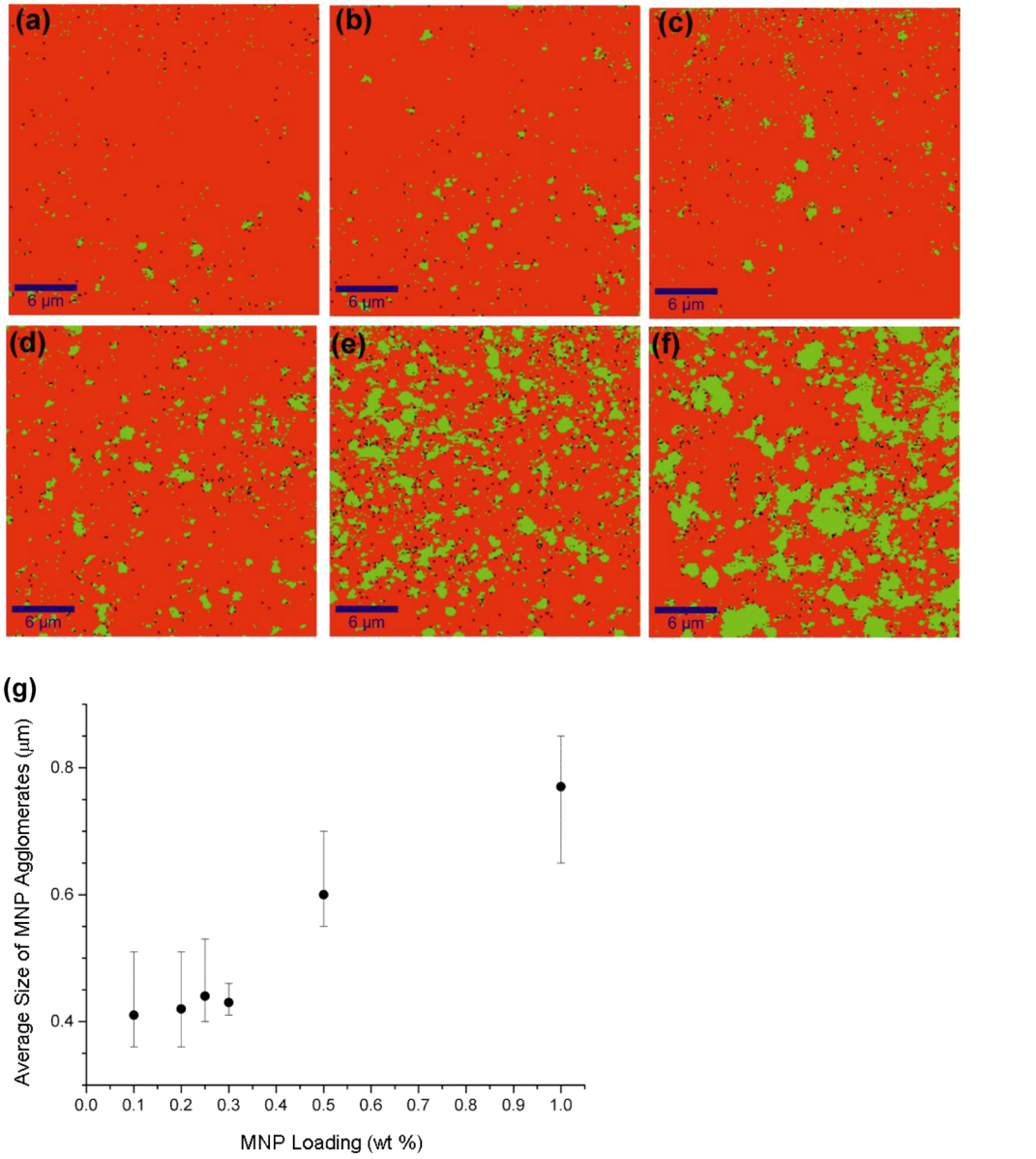

Figure 5. Dispersion of MoS_2 (green) in the epoxy matrix (red) obtained by confocal Raman imaging for specimens with MNP concentrations of (a) 0.1%, (b) 0.2%, (c) 0.25%, (d) 0.3%, (e) 0.5%, and (f) 1%. The scale bar for all images is 6 μm. (g) Quantitative analysis of the average MNP particle size as the function of the filler loading fraction. The error bars indicate the minimum and the maximum values obtained.

(<300 J/m^2). Incorporation of the MNP into the epoxy causes a large increase in the nanocomposite's G_{Ic} to ~600 J/m^2 at ~0.2% weight fraction of MNP, corresponding to a ~160% increase in the fracture energy. This improved critical energy release rate for the MNP/epoxy nanocomposite material is now comparable to that of tough polymers.[23] These results demonstrate the potency of MNP additives in toughening the baseline (brittle) epoxy material at very low nanofiller loading fraction (~0.2% by weight).

A consistent trend exhibited in the results for Young's modulus (Figure 3b), tensile strength (Figure 3c), glass transition temperature (Figure 3d), fracture toughness (Figure 4b), fracture surface roughness (Figure 4c), and fracture energy (Figure 4d) is that the MNP additives rapidly lose effectiveness beyond a loading percent of ~0.2% by weight. This warrants further investigation. To reveal the underlying mechanisms responsible for this, we generated confocal Raman spectroscopy dispersion maps (as in Figure 2b) to study the average size and distribution of the MNP agglomerates at different loading fractions. The results are shown in Figures 5a–f for the following weight fractions of MNP filler: (a) 0.1%, (b) 0.2%, (c) 0.25%, (d) 0.3%, (e) 0.5%, and (f) 1%. The red region in the dispersion maps represents the epoxy matrix, while the green regions correspond to the MNP fillers. To quantitatively compare the dispersion and agglomeration of the MNP, we divided the total area of the image exhibiting MNP Raman modes by the number of agglomerates in the image. Assuming a circular

geometry for the agglomerates, the average MNP size was estimated and is shown in Figure 5g as a function of MNP loading fraction. The plot reveals that the average MNP size increases only slightly from ~400 nm to ~420 nm in the 0−0.3% range of MNP loading. However, at higher loading fractions, the average size of the MNPs increases to ~600 nm at 0.5% loading and ~800 nm at 1% loading. This indicates that there is substantial agglomeration and clustering of the MNP fillers at loading fractions above ~0.3%, which is consistent with the reduction of the mechanical properties and the glass transition temperature (Figures 3 and 4) at these loading fractions. Filler agglomeration serves to reduce the interfacial contact area at the MNP/matrix interface and therefore diminishes the ability of the MNP to reinforce the composite. Severe agglomeration can also lead to poor adherence between the polymer matrix and the nanofillers such that the agglomerated MNPs begin to act as defect centers, which is detrimental to mechanical properties.

CONCLUSIONS

While we have demonstrated that transition metal dichalcogenide nanoplatelets can be used to significantly improve a range of mechanical properties of epoxy composites at low nanofiller loadings, there is considerable room for improvement. This creates new opportunities and possibilities for the polymer nanocomposites and 2D materials communities. We suggest two main directions for future research: (1) Exfoliation of transition metal dichalcogenides into bulk quantities of monolayer materials remains a challenge (the average thickness of MoS_2 nanoplatelets in our study was ~5−10 nm). Therefore, new and improved techniques are necessary to produce bulk quantities of monolayer transition metal dichalcogenide nanosheets that are resistant to restacking and agglomeration. (2) The dispersion in polymer matrices of pristine (*i.e.*, nonfunctionalized) transition metal dichalcogenide nanosheets is challenging above nanofiller loading fractions of ~0.2−0.3% by weight. Therefore, chemical functionalization strategies are critically important for improved dispersion and interfacial load transfer at higher nanofiller loadings. The aforementioned advances will enable transition metal dichalcogenide 2D sheets to be utilized to their maximum capacity and to achieve their full potential in polymer nanocomposites.

MATERIALS AND METHODS

Estimation of Fracture Toughness. The Mode I fracture toughness (K_{Ic}) was calculated using ASTM Standard D5045 as follows:

$$K_{Ic} = \frac{P_{max}}{BW^{1/2}} f\left(\frac{a}{W}\right)$$

where P_{max} is the maximum load on the load−displacement curve for the compact tension specimen, B is the thickness of the specimen, W is the width of the specimen, and the $f(a/W)$ term is related to the geometry of the sample. Note that in all our samples, the term a/W is equal to 0.5. For compact tension samples, f can be expressed as

$$f\left(\frac{a}{W}\right) = \left[\left(2+\frac{a}{W}\right)\left(0.886+4.64\left(\frac{a}{W}\right)-13.32\left(\frac{a}{W}\right)^2 +14.72\left(\frac{a}{W}\right)^3-5.6\left(\frac{a}{W}\right)^4\right)\right]/\left(1-\frac{a}{W}\right)^{3/2}$$

Scanning Electron Microscopy of MNP. Exfoliated MNP were characterized by scanning electron microscopy (SEM) on a Carl Zeiss Supra SEM. MNP samples were spin-coated on a silicon wafer, washed and baked to remove all traces of solvent, and imaged to determine the flake morphology.

Measurement of the Surface Roughness of the Fracture Surfaces. The arithmetic mean surface roughness (R_a) of the fracture surfaces was measured using a Dektak Surface Profiler (from Veeco). Five separate measurements were performed for each sample.

Atomic Force Microscopy (AFM) Measurements of MNP Thickness. Thickness of exfoliated MNP were characterized by atomic force microscopy Veeco Dimension 3100 AFM using a Pt coated Silicon AFM tip optimized for high sensitivity. Exfoliated MNP samples were deposited on a silicon wafer, washed and baked to remove all traces of solvent, and imaged in the contact mode to determine the average topographic height or thickness of the platelets.

Raman Spectroscopy. The Raman spectra of the exfoliated MNPs were collected using a WITec confocal Raman microscope in a backscattering configuration, utilizing a 532 nm laser as the excitation light. A 100×/0.9NA objective and a 100 μm optical fiber acting as the confocal pinhole were used for the experiments. For Raman study of the composite, we created cross sections of the composites with a low speed diamond saw. To obtain confocal Raman images, a total of 32 400 individual spectra were collected over a 30 × 30 μm^2 area of the composite. A total of three separate imagings were performed on each specimen.

Differential Scanning Calorimetry (DSC). The glass transition temperature (T_g) was measured using a PerkinElmer DSC 7. Samples of approximately 5 mg were heated in aluminum pans to 120 °C at 10 °C/min heating rate under a nitrogen purge gas. The T_g was measured on the second heating run for each sample. Multiple samples of each material were tested for statistics.

Conflict of Interest: The authors declare no competing financial interest.

Acknowledgment. N.K. acknowledges funding support from the U.S.A. National Science Foundation (Awards 1234641 and 1130215) and the John A. Clark and Edward T. Crossan Chair Professorship at the Rensselaer Polytechnic Institute.

REFERENCES AND NOTES

1. Blackman, B. R. K.; Kinloch, A. J.; Lee, J. S.; Taylor, A. C.; Agarwal, R.; Schueneman, G.; Sprenger, S. The Fracture and Fatigue Behaviour of Nano-Modified Epoxy Polymers. *J. Mater. Sci.* **2007**, *42*, 7049–7051.
2. Wetzel, B.; Rosso, P.; Haupert, F.; Friedrich, K. Epoxy Nanocomposites—Fracture and Toughening Mechanisms. *Eng. Fract. Mech.* **2006**, *73*, 2375–2398.
3. Thostenson, E. T.; Chou, T. W. Carbon Nanotube Networks: Sensing of Distributed Strain and Damage for Life Prediction and Self Healing. *Adv. Mater.* **2006**, *18*, 2837–2841.
4. Suhr, J.; Koratkar, N.; Keblinski, P.; Ajayan, P. Viscoelasticity in Carbon Nanotube Composites. *Nat. Mater.* **2005**, *4*, 134–137.

5. Zerda, A. S.; Lesser, A. J. Intercalated Clay Nanocomposites: Morphology, Mechanics, and Fracture Behavior. *J. Polym. Sci., Polym. Phys.* **2001**, *39*, 1137–1146.
6. Wang, K.; Chen, L.; Wu, J. S.; Toh, M. L.; He, C. B.; Yee, A. F. Epoxy Nanocomposites with Highly Exfoliated Clay: Mechanical Properties and Fracture Mechanisms. *Macromolecules* **2005**, *38*, 788–800.
7. Liu, W. P.; Hoa, S. V.; Pugh, M. Organoclay-Modified High Performance Epoxy Nanocomposites. *Compos. Sci. Technol.* **2005**, *65*, 307–316.
8. Stankovich, S.; Dikin, D. A.; Dommett, G. H. B.; Kohlhaas, K. M.; Zimney, E. J.; Stach, E. A.; Piner, R. D.; Nguyen, S. T.; Ruoff, R. S. Graphene-Based Composite Materials. *Nature* **2006**, *442*, 282–286.
9. Ramanathan, T.; Abdala, A. A.; Stankovich, S.; Dikin, D. A.; Herrera-Alonso, M.; Piner, R. D.; Adamson, D. H.; Schniepp, H. C.; Chen, X.; Ruoff, R. S.; *et al.* Functionalized graphene sheets for polymer nanocomposites. *Nat. Nanotechnol.* **2008**, *3*, 327–331.
10. Rafiee, M. A.; Rafiee, J.; Wang, Z.; Song, H. H.; Yu, Z. Z.; Koratkar, N. Enhanced Mechanical Properties of Nanocomposites at Low Graphene Content. *ACS Nano* **2009**, *3*, 3884–3890.
11. Rafiee, M. A.; Rafiee, J.; Srivastava, I.; Wang, Z.; Song, H. H.; Yu, Z. Z.; Koratkar, N. Fracture and Fatigue in Graphene Nanocomposites. *Small* **2010**, *6*, 179–183.
12. Naguib, M.; Kurtoglu, M.; Presser, V.; Lu, J.; Niu, J. J.; Heon, M.; Hultman, L.; Gogotsi, Y.; Barsoum, M. W. Two-Dimensional Nanocrystals Produced by Exfoliation of Ti_3AlC_2. *Adv. Mater.* **2011**, *23*, 4248–4253.
13. Ci, L.; Song, L.; Jin, C. H.; Jariwala, D.; Wu, D. X.; Li, Y. J.; Srivastava, A.; Wang, Z. F.; Storr, K.; Balicas, L.; *et al.* Atomic layers of hybridized boron nitride and graphene domains. *Nat. Mater.* **2010**, *9*, 430–435.
14. Coleman, J. N.; Lotya, M.; O'Neill, A.; Bergin, S. D.; King, P. J.; Khan, U.; Young, K.; Gaucher, A.; De, S.; Smith, R. J.; *et al.* Two-Dimensional Nanosheets Produced by Liquid Exfoliation of Layered Materials. *Science* **2011**, *331*, 568–571.
15. Butler, S. Z.; Hollen, S. M.; Cao, L. Y.; Cui, Y.; Gupta, J. A.; Gutierrez, H. R.; Heinz, T. F.; Hong, S. S.; Huang, J. X.; Ismach, A. F.; *et al.* Progress, Challenges, and Opportunities in Two-Dimensional Materials Beyond Graphene. *ACS Nano* **2013**, *7*, 2898–2926.
16. Elias, A. L.; Perea-Lopez, N.; Castro-Beltran, A.; Berkdemir, A.; Lv, R. T.; Feng, S. M.; Long, A. D.; Hayashi, T.; Kim, Y. A.; Endo, M.; *et al.* Controlled Synthesis and Transfer of Large-Area WS2 Sheets: From Single Layer to Few Layers. *ACS Nano* **2013**, *7*, 5235–5242.
17. Zhu, Y. Q.; Sekine, T.; Li, Y. H.; Wang, W. X.; Fay, M. W.; Edwards, H.; Brown, P. D.; Fleischer, N.; Tenne, R. WS_2 and MoS_2 Inorganic Fullerenes—Super Shock Absorbers at Very High Pressures. *Adv. Mater.* **2011**, *23*, 4248–4253.
18. Zhu, Y. Q.; Sekine, T.; Li, Y. H.; Fay, M. W.; Zhao, Y. M.; Poa, C. H.; Wang, W. X.; Roe, M. J.; Brown, P. D.; Fleischer, N.; *et al.* Shock-Absorbing and Failure Mechanisms of WS_2 and MoS_2 Nanoparticles with Fullerene-like Structures under Shock Wave Pressure. *J. Am. Chem. Soc.* **2005**, *127*, 16263–16272.
19. Zhang, W.; Picu, C. R.; Koratkar, N. A. The Effect of Carbon Nanotube Dimensions and Dispersion on the Fatigue Behavior of Epoxy Nanocomposites. *Nanotechnology* **2008**, *19*, 285709.
20. Zhang, W.; Suhr, J.; Koratkar, N. A. Observation of High Buckling Stability in Carbon Nanotube Polymer Composites. *Adv. Mater.* **2006**, *18*, 452–456.
21. Shojaee, S. A.; Zandiatashbar, A.; Koratkar, N.; Lucca, D. A. Raman Spectroscopic Imaging of Graphene Dispersion in Polymer Composites. *Carbon* **2013**, *62*, 510–513.
22. Schmidt, U.; Weishaupt, J.; Hollricher, O. Analysis of Multi-Component Polymer Blends with the Confocal Raman AFM. *Microsc. Microanal.* **2008**, *14*, 468–469.
23. Hull, D. *Fractography: Observing, Measuring, and Interpreting Fracture Surface Topography*; Cambridge University Press: Cambridge, 1999.
24. Arakawa, K.; Takahashi, K. Relationships between Fracture Parameters and Fracture Surface-Roughness of Brittle Polymers. *Int. J. Fract.* **1991**, *48*, 103–114.
25. Faber, K. T.; Evans, A. G. Crack Deflection Processes: 1. Theory. *Acta Metall. Mater.* **1983**, *31*, 565–576.